

# Heterogeneous ice nucleation controlled by the coupling of surface crystallinity and surface hydrophilicity

Yuanfei Bi, Raffaella Cabriolu, and Tianshu Li\*

*Department of Civil and Environmental Engineering, George Washington University, Washington, DC 20052*

E-mail: tsli@gwu.edu

## Abstract

The microscopic mechanisms controlling heterogeneous ice nucleation are complex and remain poorly understood. Although good ice nucleators are generally believed to match ice lattice and to bind water, counter examples are often identified. Here we show, by advanced molecular simulations, that the heterogeneous nucleation of ice on graphitic surface is controlled by the coupling of surface crystallinity and surface hydrophilicity. Molecular level analysis reveals that the crystalline graphitic lattice with an appropriate hydrophilicity may indeed template ice basal plane by forming a strained ice layer, thus significantly enhancing its ice nucleation efficiency. Remarkably, the templating effect is found to transit from within the first contact layer of water to the second as the hydrophilicity increases, yielding an oscillating distinction between the crystalline and amorphous graphitic surfaces in their ice nucleation efficiencies. Our study sheds new light on the long-standing question of what constitutes a good ice nucleator.

---

\*To whom correspondence should be addressed

# Introduction

In understanding and controlling the formation of ice, perhaps the most crucial question to answer is: What makes an effective ice nucleation center? The extensive studies on ice formation in supercooled cloud droplets may provide some useful insight to this question.<sup>1</sup> In clouds, the leading candidates for heterogeneous ice nucleation centers have been identified to be bacteria, pollen grains, mineral dust (e.g., clay), emission from aircraft (e.g., soot), and high-molecular-weight organic compounds (long-chain alcohols).<sup>2</sup> While general distinction exists in their chemical nature, these ice-nucleating agents share common structural features. For example, the surfaces of these substances may contain chemical groups capable of forming hydrogen bond with water. As a consequence, layers of water molecules can be hydrogen-bonded to the surfaces. The surfaces may also exhibit the ordering patterns that resemble the structure of ice. Therefore water layers bound to surfaces may be ice-like, providing template for ice to nucleate.

On the basis of laboratory experiments, general criteria for a surface to be a good ice nucleator (IN) were summarized,<sup>3</sup> and these are: (1) IN should be highly water-insoluble; (2) IN should have similar hydrogen bonds available at its surface; (3) IN should have an arrangement of atoms or molecules on its surface as close as possible to that of water molecules in some low index plane of ice. However it should be stressed that these criteria may only be suggestive but not predictive, and no unique correlation can be established between ice nucleation threshold and these surface characteristics. For example, lattice match can be a good indicator, but it cannot account for the fact that different materials with the same lattice mismatch with ice, e.g., long-chain alcohol<sup>4</sup> and lead iodide,<sup>5</sup> exhibit different freezing temperatures. Amorphous or poorly ordered materials such as soot<sup>6</sup> are also known to be effective ice nucleator, despite their non-crystalline nature. Crystalline soluble salts such as ammonium sulphate was also found to nucleate ice.<sup>7</sup> In addition, recent laboratory experiment using droplet freezing technique<sup>8</sup> further showed that non-clay mineral feldspar dominate ice nucleation in mix-phase clouds.

Here we report direct computational evidence that the crystallinity and the hydrophilicity of the carbon surface are strongly coupled to dominate the kinetics of ice nucleation. By systematically

varying the water-carbon interaction strength over a wide range and computing the ice nucleation rates explicitly, we observe a rich spectrum of heterogeneous ice nucleation behaviors on both crystalline and amorphous carbon surfaces. Remarkably, we find that only within certain ranges of hydrophilicity does the crystallinity of the carbon surface play an active role in nucleating ice, and within these ranges, crystalline carbon surface is found to be significantly more efficient than the amorphous. In other hydrophilicity, the role of crystalline ordering becomes negligible, and no appreciable difference is observed in the directly computed ice nucleation rates between the crystalline and amorphous carbon surfaces. Our study demonstrates that the commonly adopted individual criterion for good IN alone may not be sufficient for predicting the ice nucleation capacity of a surface, and points at ways of engineering surfaces for controlling ice formation.

## Methods

### Calculation of ice nucleation rate.

The direct calculation of ice nucleation rates was conducted by employing the forward flux sampling (FFS) method.<sup>9</sup> In FFS, the nucleation rate  $R$  was obtained through the product of initial flux rate  $\dot{\Phi}_{\lambda_0}$  and the growth probability  $P(\lambda_B|\lambda_0)$  (namely,  $R = \dot{\Phi}_{\lambda_0}P(\lambda_B|\lambda_0)$ ), both of which can be calculated directly by sampling the nucleation trajectories in the parameter space defined by the order parameter  $\lambda$ . The  $p_B$  histogram analysis in our previous study<sup>10</sup> has demonstrated that a good order parameter  $\lambda$  is the number of water molecules contained in the largest ice nucleus for both homogeneous and heterogeneous ice nucleation on graphitic surface. The ice-like water molecule is numerically identified by the local bond-order parameter  $q_6$  with a  $q_6 > 0.5$ .<sup>11</sup> The initial flux rate  $\dot{\Phi}_{\lambda_0}$  is obtained by  $N_0/t_0V$ , where  $N_0$  is the number of successful crossings to the interface  $\lambda_0$  from basin A, *i.e.*, the spontaneous formation of ice nucleus containing  $\lambda_0$  water molecules,  $t_0$  is the total time of initial sampling, and  $V$  is the volume. The growth probability  $P(\lambda_B|\lambda_0)$  is computed through  $P(\lambda_B|\lambda_0) = \prod_{i=1}^n P(\lambda_i|\lambda_{i-1})$ , where  $P(\lambda_i|\lambda_{i-1})$  is the crossing probability for which a trajectory starts from interface  $\lambda_{i-1}$  and ends on interface  $\lambda_i$ . By firing a large number  $M_{i-1}$  of

trial shootings from the interface  $\lambda_{i-1}$  and collecting  $N_i$  successful crossings at the interface  $\lambda_i$ , one estimates  $P(\lambda_i|\lambda_{i-1}) = N_i/M_{i-1}$ . The statistical uncertainty of  $P(\lambda_B|\lambda_0)$  consists of both the variance of binomial distributions of  $N_i$  and the landscape variance of the configurations collected at the previous interface  $\lambda_{i-1}$ .<sup>12</sup> More details of ice nucleation rate calculations by FFS can be found in Ref.<sup>10,11</sup> The computed heterogeneous ice nucleation rates for all the conditions are listed in Table S1 in Supporting Information.

## Systems.

Our molecular dynamics (MD) simulations were carried out using the monotonic-water (mW) model.<sup>13</sup> The carbon-water interaction is described based on the two-body term of the mW model. To mimic a wide range of hydrophilicity of carbon surface, the water-carbon interaction strength  $\epsilon$  is varied<sup>14–16</sup> between  $\epsilon_0$  and  $10\epsilon_0$ , where  $\epsilon_0 = 0.13$  kcal/mol is the original water-carbon interaction strength<sup>17</sup> that reproduces the experimental contact angle ( $86^\circ$ ) of liquid water on graphite. The simulations include 4096 water molecules and 1008 carbon atoms, in a nearly cubic cell combined with a periodic boundary condition (PBC). The No se-Hoover thermostat was employed to simulate the isobaric-isothermal canonical ensemble (NPT), with a relaxation time of 1 ps and 15 ps for the temperature and pressure, respectively. A time step of 5 fs is used throughout the simulations.

## Model of amorphous graphene.

To study the role of crystallinity of the carbon surface, we amorphize the graphene surface by introducing the Stone-Wales (SW) defects through the Wooten-Weaire-Winer (WWW) bond-switching Monte Carlo (MC) method.<sup>18</sup> In this approach, the carbon-carbon interaction is described by the Keating-like potential:<sup>19</sup>

$$V = \sum_{i,j} \frac{k}{2} [r_{ij}^2 - r_0^2]^2 + \sum_{i,j,k} h \left[ \vec{r}_{ki} \cdot \vec{r}_{kj} + \frac{r_0^2}{2} \right]^2, \quad (1)$$

where  $r_0 = 1.42 \text{ \AA}$  which denotes the equilibrium C-C bond length. The first and second terms of the potential describe the energies for bond stretching and bond bending, with  $k=7.5 \text{ kcal/mol}$  and  $h$  ( $h/k = 0.2$ ) being the corresponding spring constants, respectively. The MC simulation includes two types of moves: a single particle displacement and a WWW bond-switching move. The latter move allows introducing five- and seven-fold rings in the graphene sheet while preserving the local three fold coordination of carbon atoms. The schematic diagram for the bond-switching move is shown in Fig. 1. By progressively introducing the bond-switching move, one may disrupt the translational symmetry of the graphene while minimizing the coordinational defect. In our procedure of amorphizing graphene, each MC step consists of one attempt of single particle displacement and one bond-switching move, both performed randomly throughout the graphene sheet. The standard Metropolis MC procedure was employed. To allow the structure to relax sufficiently, particularly once the bond-switching move is accepted, the single particle move and the bond-switching move are performed at  $k_B T = 0.33 \text{ eV}$  and  $39 \text{ eV}$ , respectively. After  $10^9$  MC steps, the structure was quenched at  $k_B T = 0.033 \text{ eV}$  for obtaining realistic atomic structure for amorphous graphene at room temperature. Fig. 1 (b)&(c) show the distributions of the C-C bond length and C-C-C bond angle of the amorphous graphene. The topology analysis shows the amorphous graphene network is composed of 35% pentagons, 37% hexagons, 22% heptagons, and 4.9% octagons, in agreement with the ring statistics (34.5%, 38% 24%, and 4.5%, respectively) obtained by Kapko *et. al.*<sup>20</sup>

## Results and Discussion

We first carried out study of heterogeneous ice nucleation on carbon surface with the original water-carbon interaction strength ( $\epsilon = \epsilon_0$ ). Figure 2a shows the computed heterogeneous ice nucleation rates on both crystalline and amorphous graphene. At both temperatures investigated, no distinguishable difference is found on the computed ice nucleation rate between the two surfaces. The result may appear surprising in its first glimpse but can be understood by the fact that crystalline graphene neither binds water nor templates ice. In fact the heterogeneous ice nucle-

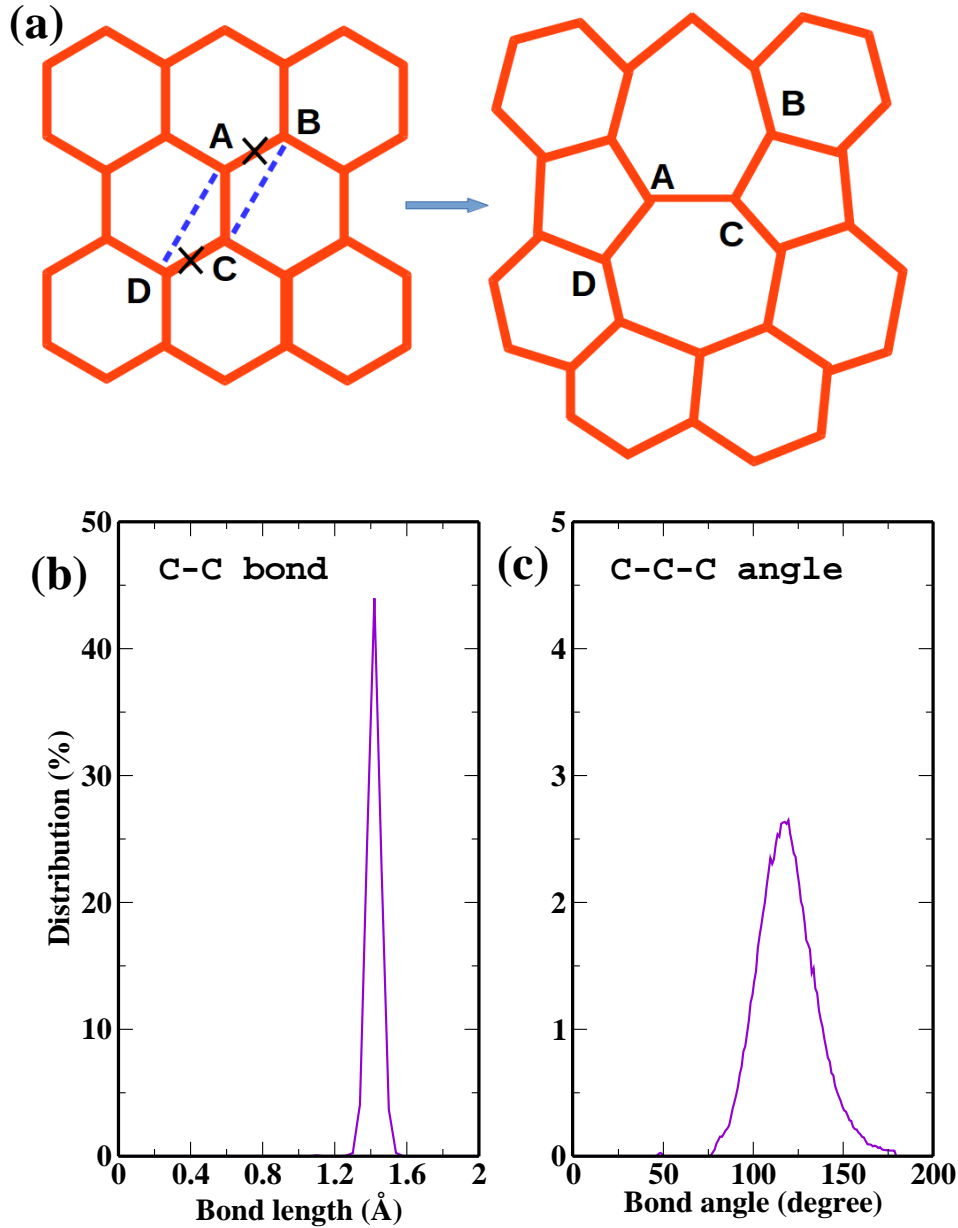


Figure 1: (a) Bond interchange using the WWWW algorithm to introduce the Stone-Wales defect in graphene. The SW defect is generated by rotating a carbon-carbon bond by 90 degrees. Within the WWWW framework, this is achieved by first randomly selecting a bond, *e.g.*, AC, followed by a random selection of two carbon atoms connecting to A and C, respectively, but on the opposite sides of bond AC, *e.g.*, atom B and D. Then the bond AB and CD are replaced by new bonds AD and BC (dashed lines). The final amorphous graphene structure yields a distribution of the carbon-carbon bond length (b) and the carbon-carbon-carbon bond angle (c).

ation of graphene was recently attributed to the induced layering of water density perpendicular to water-carbon interface:<sup>14,16,17</sup> Since the oscillation of water density near the water-carbon interface matches well the density profile of ice, and the motion of water molecules in the contact layers is well restricted within the plane, the space that these water molecules can explore, hence the entropic barrier of ice nucleation, is effectively reduced. It has been further suggested<sup>16</sup> that water molecules in the first layer experience a nearly uniform potential from graphene. In other words, water molecules in contact layers see carbon surface as an atom-less flat surface. Indeed, our calculated density of water (Fig. 2b) shows that the absence of crystallinity in graphene does not alter the profiles of water density normal to the surface. This is consistent with the observed insensitivity of ice nucleation rate on surface crystallinity under the original surface hydrophilicity.

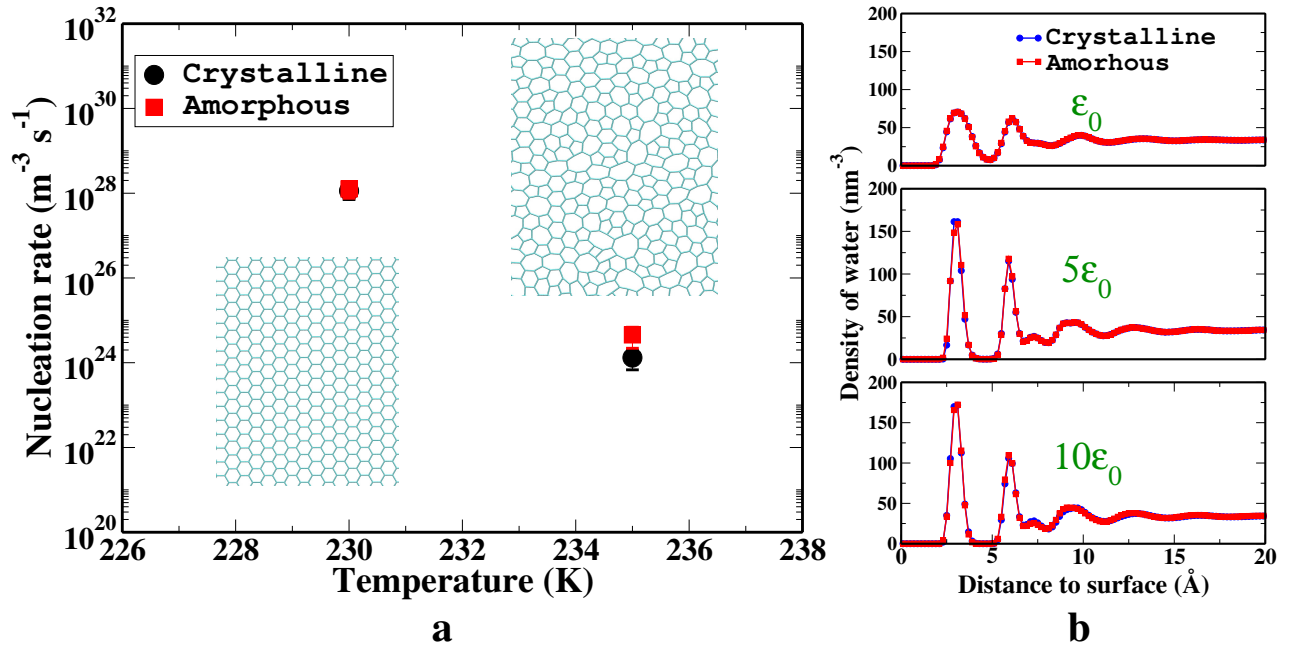


Figure 2: (a) Calculated heterogeneous ice nucleation rates on crystalline and amorphous graphene at 230 K and 235 K. Inset shows the atomic structures of both crystalline and amorphous graphene. (b) Calculated density profiles of water along the direction normal to the water-graphene interface, for different water-carbon interaction strengths.

The interesting results are obtained when water-carbon interaction strength  $\epsilon$  is allowed to vary. Increasing  $\epsilon$  makes carbon atoms bind water more strongly, and correspondingly the surface becomes more hydrophilic. As shown in Figure 3, the variation of  $\epsilon$  (hence hydrophilicity)

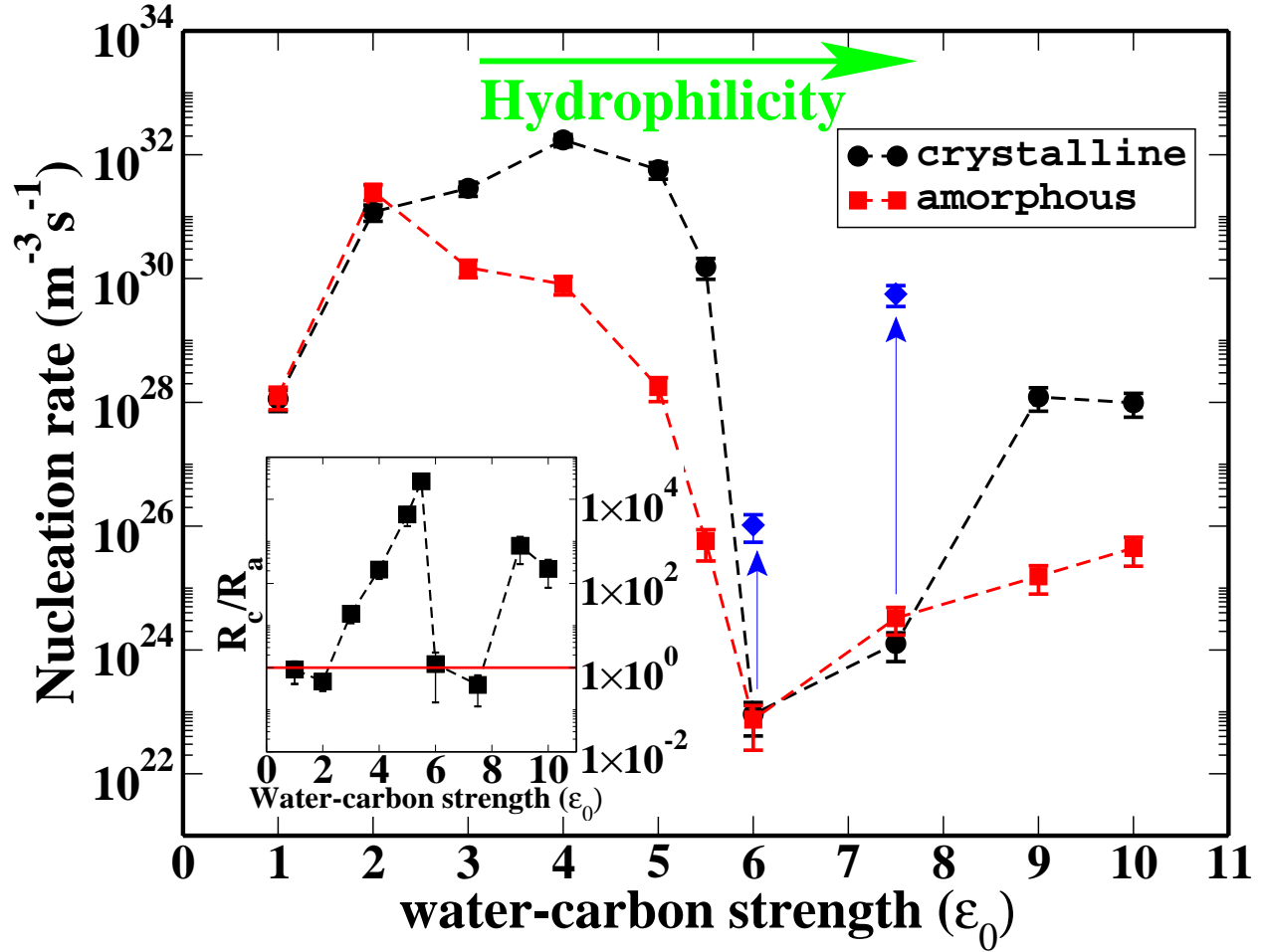


Figure 3: Variation of the calculated ice nucleation rates with water-carbon interaction strength  $\epsilon$  (in the unit of the original strength  $\epsilon_0$ ) at 230 K, for both crystalline and amorphous graphene. The blue diamonds indicate the calculated nucleation rate of ice forming on crystalline graphene with a stretched carbon-carbon bond length of  $1.46 \text{ \AA}$ . Inset shows the ratio of the ice nucleation rates between the crystalline and amorphous graphene  $R_c/R_a$ , as a function of water-carbon strength. The red horizontal line indicates a ratio of one.



yields a rich spectrum of heterogeneous ice nucleation behaviors on both crystalline and amorphous graphene. First, increasing surface hydrophilicity initially enhances the ice nucleation rates on both surfaces, which maximizes the ice nucleation efficiencies for the crystalline and amorphous at the water-carbon strength of  $4\epsilon_0$  and  $2\epsilon_0$ , respectively. A further increase of hydrophilicity, nevertheless, starts weakening the ice nucleation capacities of both surfaces, until the minimum nucleation rates are reached at  $6\epsilon_0$  for both surfaces. Upon additional enhancement of hydrophilicity, both surfaces are found to re-gain their abilities of nucleating ice.

Remarkably, in contrast to the behaviors observed at the original water-carbon strength  $\epsilon_0$ , the crystallinity of the graphene surface was found to play a significant role in facilitating ice nucleation when surface hydrophilicity is varied. As shown in Figure 3, there exist ranges of hydrophilicity where the crystalline graphene yields significantly higher ice nucleation rate than the amorphous graphene. This can be better illustrated by the inset of Fig. 3 which shows the ratio of the ice nucleation rate resulted from the crystalline graphene to that of the amorphous surface,  $R_c/R_a$ , as a function of water-carbon interaction strength  $\epsilon$ . It is evident that within the low ( $\epsilon \leq 2\epsilon_0$ ) and mid-high ( $6\epsilon_0 \leq \epsilon \leq 7.5\epsilon_0$ ) ranges of water-carbon interaction strength, the crystalline graphene shows no appreciable difference from the amorphous in its ice nucleation ability, whereas it becomes much more efficient within other ranges. In particular, at  $\epsilon = 5\epsilon_0$  the crystalline graphene yields an ice nucleation rate almost  $10^5$  times higher than the amorphous, strongly suggesting that the crystallinity is a key factor for ice nucleation under such hydrophilicity.

The results immediately suggest the existence of a coupling resulted from the two surface characteristics that dictates ice nucleation, and that the coupling strength varies non-monotonically with the surface hydrophilicity. To understand the origin of this coupling behavior, we first examine the recently proposed layering mechanism. Fig. 2b shows, however, that the density profile of water normal to the carbon-water surface is essentially insensitive to the change of surface crystallinity, within the entire range of hydrophilicity investigated in this work. Clearly, the observed difference of ice nucleation rates induced by crystallinity may not be explained by the layering mechanism.

To shed light on its origin, we examine the structure of the critical ice nucleus forming on car-

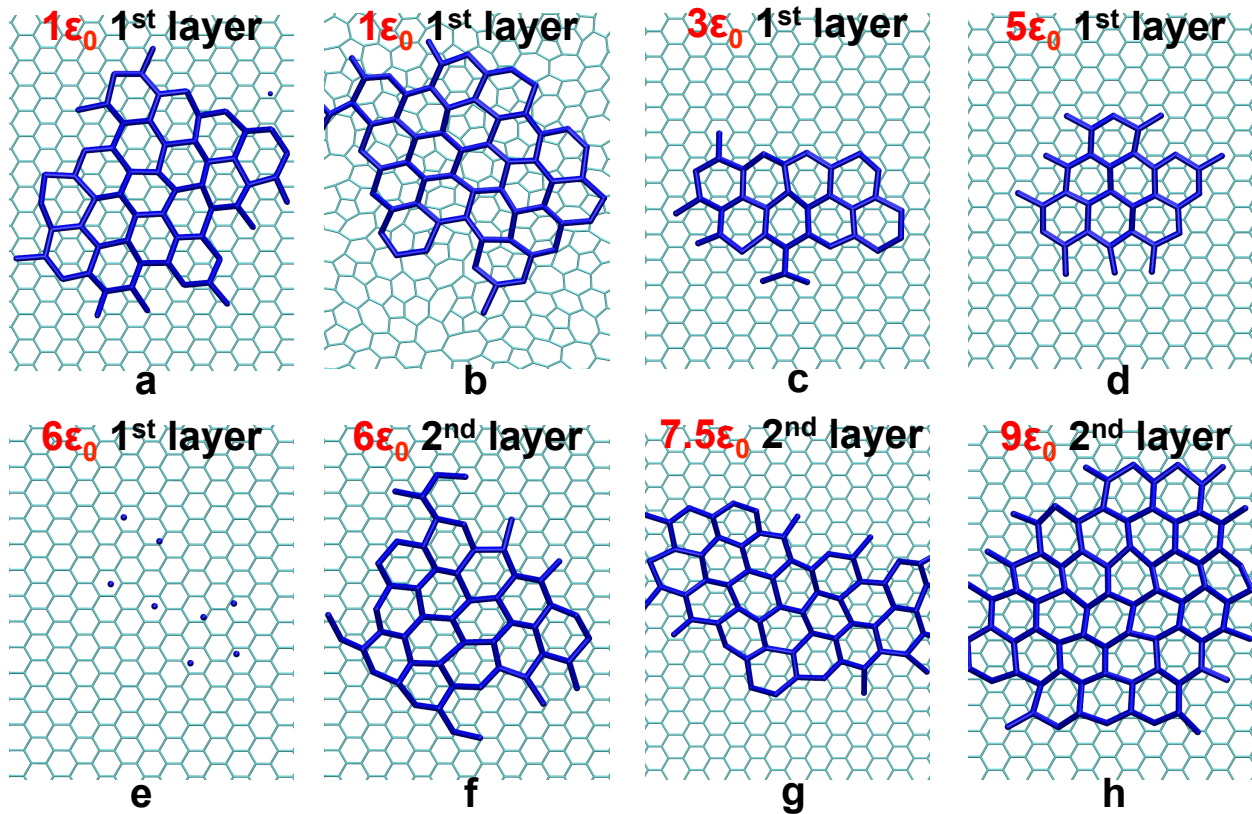


Figure 4: Evolution of ice layer (blue) in the critical nucleus forming on graphene (cyan) with water-carbon interaction strength  $\epsilon$ . (a) and (b) show the ice layer forming in the first contact layer of water on the crystalline and the amorphous graphene, respectively, at the original strength  $\epsilon_0$ . With an increasing  $\epsilon$ , the ice layer gains lattice registry with respect to the crystalline graphene, as in (c) and (d). Further hydrophilicity increase disfavors ice formation in the first contact layer, as in (e) where only dangling water molecules appear, and instead, facilitates ice nucleation in the second contact layer, as in (f). The ice layer gradually aligns registered with the crystalline graphene with the continuous increase of water-carbon strength, as in (h).

bon surface. As heterogeneous ice nucleation aligns the basal plane of ice parallel to graphene, the ice structure in the contact layers are expected to play an active role in ice nucleation. Fig. 4a & b show the structure of the first ice layer of a critical nucleus formed on the underlying substrate with the original  $\varepsilon = \varepsilon_0$ , for both crystalline and amorphous graphene. As expected, the basal plane of ice does not appear to match the underlying crystalline graphene lattice. Correspondingly the computed ice nucleation rates do not exhibit fundamental difference when the crystallinity of graphene changes. As the water-carbon strength increases to  $3\varepsilon_0$ , the first layer of ice and the graphene lattice are found to form a nearly commensurate structure, *i.e.*, each six member ring of water encloses a six member ring of carbon, as shown in Fig. 4c. On the basis of the underlying crystalline graphene lattice, the pseudo commensurate structure can be considered as a  $3 \times 3$  supercell, containing three graphene unit cells along each direction. We note that at this hydrophilicity, the crystalline graphene already yields an ice nucleation rate about ten times higher than that of the amorphous graphene. As shown in Fig. 4d, the pseudo commensurate structure becomes even more evident at  $5\varepsilon_0$ , but interestingly, disappears upon a further increase of water-carbon strength to  $6\varepsilon_0$ . Under this hydrophilicity ( $6\varepsilon_0$ ), it is found that the water molecules in the first contact ice layer no longer arrange themselves into an ice like structure (Fig. 4e). Instead, the basal plane of ice forms in the second layer of water, and it is further observed that the second ice layer, similar to the *first* ice layer forming at the original water-carbon strength  $\varepsilon_0$ , is incommensurate with the underlying graphene lattice (Fig. 4f). We also note that at this water-carbon strength ( $6\varepsilon_0$ ), the computed ice nucleation rates for both crystalline and amorphous graphene become equivalent again, and reach their minima (see Fig. 3). More interestingly, upon a further increase in hydrophilicity, *e.g.*,  $\varepsilon = 9\varepsilon_0$ , the basal plane of ice in the second layer appears to form the  $3 \times 3$  pseudo commensurate structure, similar to the first ice layer formed on the crystalline graphene at  $3\varepsilon_0 \sim 5\varepsilon_0$ . Through the formation of the pseudo commensurate structure, the crystalline graphene now regains its efficiency for promoting ice nucleation.

The molecular analysis of ice nucleus suggests that the higher ice nucleation efficiency of the crystalline graphene within  $2\varepsilon_0 \leq \varepsilon \leq 6\varepsilon_0$  and  $\varepsilon \geq 7.5\varepsilon_0$  is closely related to its ability of forming

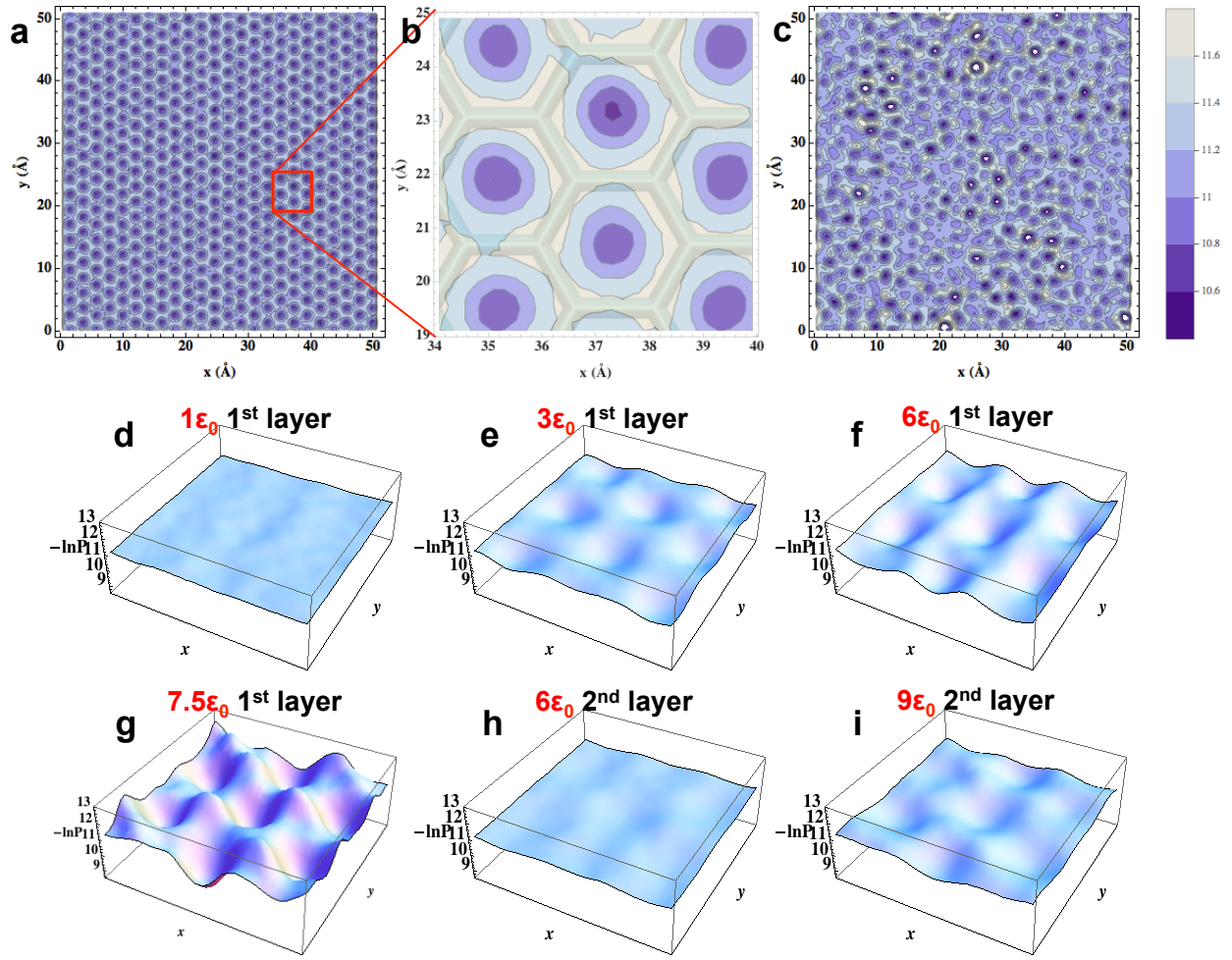


Figure 5: The in-plane distribution of water molecules in the contact layers of graphene at 230 K. For clarity, the distribution is defined as  $-\ln[P(x,y)]$ ,<sup>16</sup> where  $P(x,y)$  is the probability density of finding a water molecule located at  $(x,y)$  in the plane. (a) and (c) show the contour of  $-\ln[P(x,y)]$  computed for the first water layers in contact with crystalline graphene and amorphous graphene, respectively, with a carbon-water strength of  $\epsilon = 3\epsilon_0$ . As indicated by the contour legend, a darker color represents a higher probability of distribution. (b) is the zoom-in of a local region in (a), which shows water tends to be adsorbed above the center of carbon hexagonal ring. To demonstrate the influence of water-carbon interaction strength  $\epsilon$  on the distribution of water in contact layers, (d)~(i) show the distribution  $-\ln[P(x,y)]$  as a function of both  $x$  and  $y$  for the same region as in (b), with different hydrophilicity. In general, the increasing hydrophilicity of crystalline graphene patterns the first layer of water, which resembles the underlying graphene lattice. When water-carbon strength is high enough (as in (i)), the second layer of water is also patterned, as a result of the strong localization of water in the adsorption sites in the first layer and the local tetrahedral ordering of water.

an ice layer nearly commensurate with the underlying graphene lattice. Essentially this can be understood on the basis of the templating effect, albeit that the templating of ice occurs over the supercell of graphene lattice. The question now is: why does this templating effect only occur at certain hydrophilicity?

To answer this question, we examine the in-plane density of water in the contact layers of graphene. At a low water-carbon strength, *i.e.*, when carbon atom binds water weakly, water molecules in the first contact layer only experiences a nearly uniform potential from the underlying graphene. This can be illustrated by the in-plane distribution of water density in Fig. 5d. When carbon binds water more strongly ( $\epsilon \geq 3\epsilon_0$ ), the in-plane density distribution of water in the first layer begins affected by the underlying atomic structures. In the case of crystalline graphene, water molecules in the contact layer are found to preferentially locate themselves above the center of the carbon hexagonal ring (see Fig. 5b), making those weak adsorption sites of water. Consequently, the density of water clearly displays a pattern reminiscent to graphene lattice, as shown in Fig. 5a. The ordering of water density in the first layer, which partially matches the ice basal plane of ice, thus may effectively increase the possibility of forming an ice-like fragment. In the case of amorphous graphene, the disordered, less uniform water density in the first layer (Fig. 5c) in fact frustrates the crystalline ordering required for ice nucleation, which leads to a decrease of ice nucleation rate. As a consequence, the difference in the ice nucleation efficiency between a crystalline and amorphous graphene starts increasing with hydrophilicity.

As water-carbon interaction becomes even stronger (*e.g.*,  $6\epsilon_0$ ), the water molecules in the first layer are further constrained around the adsorption sites (Fig.5f). This leads to two effects that both suppress ice nucleation on crystalline graphene surface. First, because the formation of the hexagonal ice patchworks on crystalline graphene requires that only two thirds of the adsorption sites are filled while the rest one third are empty (see Fig. 4c & d), a full coverage of water with strong binding strength in fact structurally hinders ice nucleation.<sup>16</sup> Second, since the underlying graphene structure is rigid with a fixed carbon-carbon bond length  $d_{CC} = 1.4 \text{ \AA}$ , the formation of an ideal commensurate superstructure that matches both ice and graphene would require an

in-plane lattice constant of ice of  $4.2 \text{ \AA}$ , *i.e.*, three times of  $d_{CC}$ . This implies that the ice layer in such structure must be strained (compressed in this case), given that the equilibrium in-plane lattice constant of ice is  $4.5 \text{ \AA}$ . Therefore the strain energy cost of imposing such perfect match eventually makes the formation of the strained ice layer energetically unfavorable in the contact layer. To further demonstrate the role of strain, we increase the carbon-carbon bond length in crystalline graphene to  $1.46 \text{ \AA}$ , in order to better match ice lattice. The calculated ice nucleation rate at both  $6\epsilon_0$  and  $7.5\epsilon_0$  indeed show that the elongated crystalline graphene yields significant enhancement on ice nucleation rate (Fig. 3) relative to those of the unstrained graphene.

As the first water layer becomes inactive, the nucleation of ice consequently starts occurring in the second layer of water when  $\epsilon \geq 6\epsilon_0$ . In this case, as the in-plane water density in the second layer is nearly uniform (Fig. 5h), the crystallinity of the underlying graphene becomes inactive again in ice nucleation, as evidenced by the synchronization of the computed ice nucleation rates within  $6\epsilon_0 \leq \epsilon \leq 7.5\epsilon_0$ . Interestingly, a further increase of hydrophilicity ( $\epsilon \geq 9\epsilon_0$ ) is found to nearly immobilize water molecules within the first water layer in their adsorption sites. The strong localization of water in the first water layer essentially turns it into an image of the underlying crystalline graphene sheet. The second layer of water, now under the influence of the patterning from the first layer and the water-water interaction, becomes also structured (Fig. 5i) and tends to facilitate the formation of the commensurate ice-like structure. In other words, the first and the second layers of water at the high hydrophilicity act almost as the graphene substrate and the first layer of water at the low hydrophilicity, respectively. In this way, the crystalline graphene sheet gains renewed ice nucleation capability, making it again superior than amorphous graphene for nucleating ice.

The findings in this work have a few important implications regarding our understanding of heterogeneous ice nucleation. Perhaps the most immediate implication is that neither surface crystallinity nor surface hydrophilicity alone may be a good indicator for the ice nucleation efficiency of a surface. Instead, the combined surface characteristics may yield a complex coupling that dominates ice nucleation behaviors. This may potentially explain why materials that have similar lattice

mismatch with ice exhibit drastically different ice nucleation behaviors, and that no correlation has been established between ice nucleation threshold and any of the crystallographic characteristics.<sup>3</sup> Therefore a thorough understanding of the ice nucleation capacity for an IN should be achieved through a comprehensive study by explicitly considering all the necessary molecular details at the surface. Second, it is envisioned that the surface chemistry and surface crystallinity may also be coupled with the elasticity of the substrate. In our modeling the graphene surface is considered rigid. This is a good approximation as carbon-carbon bond is much stronger than the hydrogen bond of ice. When ice nucleates on a soft substrate that has a shear modulus lower than or comparable to that of ice, the possible local deformation of the substrate should play an active role if there exists a lattice mismatch between ice and the surface. Since a soft substrate may better template ice for a lower strain energy cost, the range of its lattice mismatch can be wider than a stiff substrate for achieving the comparable ice nucleation efficiency. This also may explain why some soft materials, *e.g.*, self-assembled monolayers of amphiphilic alcohols,<sup>4</sup> are known as the most effective INs.<sup>1</sup>

## Acknowledgment

The work is supported by NSF through award CMMI-1537286. T. L. also thanks the Sloan Foundation through the Deep Carbon Observatory for supporting this work.

## References

- (1) Murray, B. J.; O’Sullivan, D.; Atkinson, J. D.; Webb, M. E. Ice nucleation by particles immersed in supercooled cloud droplets. *Chem. Soc. Rev.* **2012**, *41*, 6519–6554.
- (2) Cantrell, W.; Heymsfield, A. Production of ice in tropospheric clouds: A review. *B Am Meteorol Soc* **2005**, *86*, 795–807.

- (3) Pruppacher, H.; Klett, J. *Microphysics of Clouds and Precipitation*; Kluwer Academic Publisher, 2007.
- (4) Popovitz-Biro, R.; Wang, J. L.; Majewski, J.; Shavit, E.; Leiserowitz, L.; Lahav, M. Induced freezing of supercooled water into ice by self-assembled crystalline monolayers of amphiphilic alcohols at the air-water interface. *Journal of the American Chemical Society* **1994**, *116*, 1179–1191.
- (5) Bryant, G. W.; Hallett, J.; Mason, B. J. The epitaxial growth of ice on single-crystalline substrates. *J Phys Chem Solids* **1960**, *12*, 189–195.
- (6) Popovicheva, O.; Kireeva, E.; Persiantseva, N.; Khokhlova, T.; Shonija, N.; Tishkova, V.; Demirdjian, B. Effect of soot on immersion freezing of water and possible atmospheric implications. *Atmospheric Research* **2008**, *90*, 326–337.
- (7) Zuberi, B.; Bertram, A. K.; Koop, T.; Molina, L. T.; Molina, M. J. Heterogeneous Freezing of Aqueous Particles Induced by Crystallized (NH<sub>4</sub>)<sub>2</sub>SO<sub>4</sub>, Ice, and Letovicite. *J Phys Chem A* **2001**, *105*, 6458–6464.
- (8) Atkinson, J. D.; Murray, B. J.; Woodhouse, M. T.; Whale, T. F.; Baustian, K. J.; Carslaw, K. S.; Dobbie, S.; O’Sullivan, D.; Malkin, T. L. The importance of feldspar for ice nucleation by mineral dust in mixed-phase clouds. *Nature* **2013**, *498*, 355–358.
- (9) Allen, R. J.; Frenkel, D.; Wolde, P. R. T. Simulating Rare Events in Equilibrium or Nonequilibrium Stochastic Systems. *J. Chem. Phys.* **2006**, *124*, 024102 1–16.
- (10) Cabriolu, R.; Li, T. Ice nucleation on carbon surface supports the classical theory for heterogeneous nucleation. *Physical Review E* **2015**, *91*, 052402.
- (11) Li, T.; Donadio, D.; Russo, G.; Galli, G. Homogeneous Ice Nucleation from Supercooled Water. *Phys Chem Chem Phys* **2011**, *13*, 19807–19813.



- (12) Allen, R. J.; Frenkel, D.; Wolde, P. R. T. Forward Flux Sampling-type Schemes for Simulating Rare Events: Efficiency Analysis. *J. Chem. Phys.* **2006**, *124*, 194111 1–17.
- (13) Molinero, V.; Moore, E. B. Water Modeled As an Intermediate Element between Carbon and Silicon. *J Phys Chem B* **2009**, *113*, 4008–4016.
- (14) Lupi, L.; Molinero, V. Does hydrophilicity of carbon particles improve their ice nucleation ability? *J Phys Chem A* **2014**, *118*, 7330–7337.
- (15) Cox, S. J.; Kathmann, S. M.; Slater, B.; Michaelides, A. Molecular simulations of heterogeneous ice nucleation. I. Controlling ice nucleation through surface hydrophilicity. *J Chem Phys* **2015**, *142*, 184704.
- (16) Cox, S. J.; Kathmann, S. M.; Slater, B.; Michaelides, A. Molecular simulations of heterogeneous ice nucleation. II. Peeling back the layers. *J. Chem. Phys.* **2015**, *142*, 184705.
- (17) Lupi, L.; Hudait, A.; Molinero, V. Heterogeneous Nucleation of Ice on Carbon Surfaces. *J Am Chem Soc* **2014**, *136*, 3156–3164.
- (18) Wooten, F.; Winer, K.; Weaire, D. Computer Generation of Structural Models of Amorphous Si and Ge. *Phys Rev Lett* **1985**, *54*, 1392–1395.
- (19) Keating, P. N. Effect of invariance requirements on the elastic strain energy of crystals with application to the diamond structure. *Physical Review* **1966**, *145*, 637.
- (20) Kapko, V.; Drabold, D. A.; Thorpe, M. F. Electronic structure of a realistic model of amorphous graphene. *phys. stat. sol. (b)* **2010**, *247*, 1197–1200.